Detection Threshold and Location Resolution of the Alberta Geological Survey Earthquake Catalogue

by Ryan Schultz, Virginia Stern, Yu Jeffrey Gu, and David Eaton

INTRODUCTION

The Western Canada Sedimentary Basin (WCSB) is a low seismicity area, with fewer than fifteen cataloged $M_L > 3.5$ events since 1985 (Earthquakes Canada, 2013b). Since 1918, there have been more than 800 earthquakes reported in this region (Earthquakes Canada, 2013b), mainly clustered near the town of Rocky Mountain House (Rebollar *et al.*, 1982, 1984; Wetmiller, 1986), the Brazeau River (Schultz *et al.*, 2014), Fort St. John (Horner *et al.*, 1994), Turner Valley, Kinbasket Lake (Ellis and Chandra, 1981), and the Horn River Basin (BC Oil and Gas Commission, 2012); a single event larger than M_L 4.5 was also reported near Snipe Lake (8 March 1970, 18:52:18 UTC; see Milne, 1970). The most active of these clusters is in the Strachan D-3A gas field near Rocky Mountain House, where 146 events were recorded over a span of 23 days in 1980 (Wetmiller, 1986). Many of these aforementioned clusters have been conjectured as induced by gas extraction (Baranova *et al.*, 1999), waste water disposal (Horner *et al.*, 1994; Schultz *et al.*, 2014), or hydraulic fracturing operations (BC Oil and Gas Commission, 2012; Farahbod *et al.*, 2014).

Historically, the compilation of the Earthquakes Canada Catalogue (EqCC) has been the responsibility of Natural Resources Canada (NRCan). More recently, a new initiative was taken by the Alberta Geological Survey (AGS) to improve the earthquake catalog in an effort to better understand the tectonics and seismicity of Alberta (AB). Interested readers are referred to Stern *et al.* (2013) for specific details on the methodology, station parameters, and earthquake locations of the AGS catalog. Overall, the quality and density of documented earthquakes is subject to the performance of the recording array (Fig. 1). Similar to the EqCC, the AGS catalog includes continuous waveform data from the Canadian National Seismic Network (CNSN); however, the AGS catalog is supplemented by continuous waveform data from the Canadian Rockies and Alberta Network (CRANE, see Gu *et al.*, 2011), the Alberta Telemetered Seismic Network (ATSN, see Eaton, 2014), and the Montana Regional Seismic Network (MRSN, see D'Alessandro and Stickney, 2012). The majority of stations utilized in this study are broadband, for instance CRANE and ATSN stations are composed entirely of Nanometrics Trillium Compacts, 120s, and 240s. Most CNSN stations are broadband with Güralp CMG-3Ts, -3NSNs, and -3ESPs, with the exception of a few short period Geotech S13s. Finally, the MRSN stations utilized during this study are predominantly short-period Kinemetrics EpiSensor ES-Ts and Mark Products L-4Cs, whereas the station EGMT records with a Streckeisen STS-2. CRANE, which is unavailable to NRCan as it is nontelemetered, initiates our supplementary data in late 2006 when the University of Alberta began the installation and maintenance of their seismic network. In total, the availability of more than 30 additional seismic monitoring stations provides an increased capacity to constrain event hypocenters and enriches the earthquake catalog in AB and the surrounding area (Fig. 2). The ongoing investigation in this region highlights the need for an improved understanding of small-to-medium earthquakes and their relationship to the recording network's performance.

In this paper, we quantify the performance differential between the EqCC and our enriched catalog as a result of additional receiver density. Because of the relative quiescence of the WCSB, the origins of epicenter resolution and the limitations of network performance are explored by performing synthetic tests. First, the ambient noise characteristics at individual stations are quantitatively analyzed to constrain their spectral and temporal variations. For many stations the dominant source of noise relevant to earthquake bandwidth is anthropogenic in origin, showing strong diurnal, weekly, and seasonal variations (up to 30 dB variability). The results from ambient noise analysis are combined with simulation of earthquake spectra to quantify station and network performance. These synthetic calculations determine the spatial variation of noise characteristics, magnitude of completeness (M_c), and epicenter resolution. Next, we empirically determine M_c at cluster locations where data have been sufficiently cataloged and compare to the simulated results. Finally, we forward model epicenter resolution based on estimates of picking error. Our findings provide a metric for the performance of the AGS catalog and a blueprint for future improvements to regional seismic monitoring and analysis in the WCSB.

NOISE CHARACTERIZATION

Ambient seismic noise plays a major part in determining the reliability of hypocenter inversions. Seismic noise is often characterized by its source: high-frequency oscillations show

doi: 10.1785/0220140203

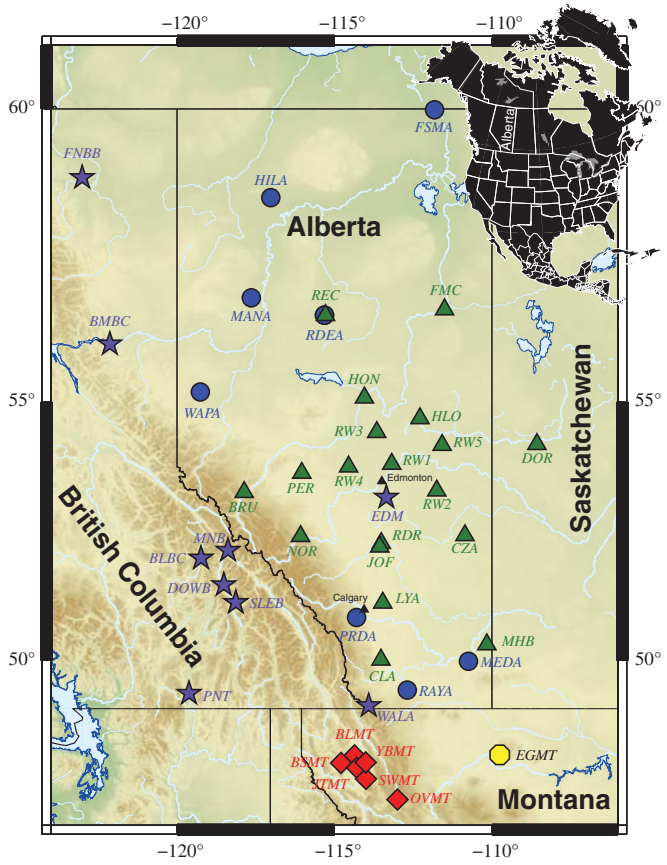

▲ **Figure 1.** Locations of seismic stations used in this study: 19 Canadian Rockies and Alberta Network (CRANE) stations (green triangles), 10 Canadian National Seismic Network (CNSN) stations (purple stars), 9 Alberta Telemetered Seismic Network stations (blue circles), 6 Montana Regional Seismic Network stations (red diamonds), and 1 USArray station (yellow octagon). The CNSN station YKW3 (~15 km north of Great Slave Lake) is not shown in this figure. Major cities are labeled with black triangles. Inset map shows the location of Alberta (AB) in the context of North America.

strong diurnal variations and are typically indicative of cultural noise, whereas ubiquitous long-period noise has been shown to result from the coupling of ocean waves to the crust and wave–wave interference (Longuet-Higgens, 1950; Hasselmann, 1963; Webb, 2007). Furthermore, interactions between wind (Withers *et al.*, 1996; Young *et al.*, 1996; De Angelis and Bodin, 2012) and local flora or topography as well as persistent, flowing water (Burtin *et al.*, 2008, 2010; Tsai *et al.*, 2012) or large lakes (Koper *et al.*, 2009; Gu and Shen, 2012) have been suggested to act as pervasive sources of noise.

In our study, we utilize the software PQLX (McNamara and Buland, 2004; McNamara and Boaz, 2011) to assess the seismic noise of all available data during our study period. Continuous waveform data for all networks and stations are segmented into one hour intervals, which are allowed to overlap by 50%, and are then transformed to acceleration power spectral density (PSD) plots. PSDs calculated in this manner are a robust estimate (error of −2.14 to +2.87 dB) of the spectral content of stationary noise. The time variability of noise is accounted for by an accumulation of PSDs over multiple intervals, which is often analyzed as a statistical distribution known as a probability distribution function (PDF).

PDFs of waveform data (Figs. 3 and 4) enable us to assess ambient site conditions, patterns in noise spectrum, and the overall performance of a given station. The most consistent feature among all stations PDFs is an increase in noise similar to the new low-noise model (NLNM, see Peterson, 1993) from 1 to 20 s. Noise within this frequency range is predominantly contributed by microseisms and will be referred to as the microseism band (MB). Two peaks are observed within the MB: a high amplitude, shorter period peak at 4–6 s and a less energetic, longer period peak at 10–15 s. The origin of this noise source is well studied, the former peak (4–6 s) is due to the generation of standing gravity waves from superposition of oceanic waves with the same frequency, propagating in opposite directions (Longuet-Higgens, 1950), whereas the latter (10–15 s) arises from the conversion of ocean wave energy to seismic energy at the shore or ocean shelf as well as other nonlinear wave interactions (Hasselman, 1963).

At longer periods (LP; > 20 s), stations with Trillium 120 and 240s (Fig. 3) perform consistently well, with modal noise values closely tracking the NLNM up to a period of ~50 s; deviations from the NLNM at even longer periods are due to instrument self noise (e.g., ~ − 170 dB at 100 s for the Trillium 240s). The lack of significant diurnal variations within this frequency band suggests that vault construction and location are adequate for thermal and barometric insulation (Beauduin *et al.*, 1996; Diaz *et al.*, 2010). A similar trend is observed in the Redwater deployments (RWX, Fig. 4), albeit with higher overall noise due to the larger self noise associated with Trillium Compacts installed in these stations (with the exception of RW1, which was installed with a 120). Exceptionally large amplitude noise observed as the skew in PSD distributions is accounted for by the long-period component of surface waves from teleseisms because PQLX does not differentiate between earthquake and noise recordings. It is noted that PSDs calculated for the horizontal components are well correlated with the noise profiles of their vertical counterparts for most frequency bands. However, at LP (> 20 s) the horizontal components exhibit a more diffuse distribution of noise with higher overall amplitudes (~25 dB difference). These results are consistent with observations of seismic recordings of ground rotation as a result of atmospheric pressure fluctuations (e.g., De Angelis and Bodin, 2012). Despite the use of small and rounded surface profiles in an effort to minimize wind coupling, residual effects of wind still manifest into modest surface tilt in the horizontal PDFs. The attenuation of the surface tilt would require installation on bedrock or more costly vault constructions, that is, borehole deployments buried at hundreds of meters of depth, which is impractical in much of the AB WCSB.

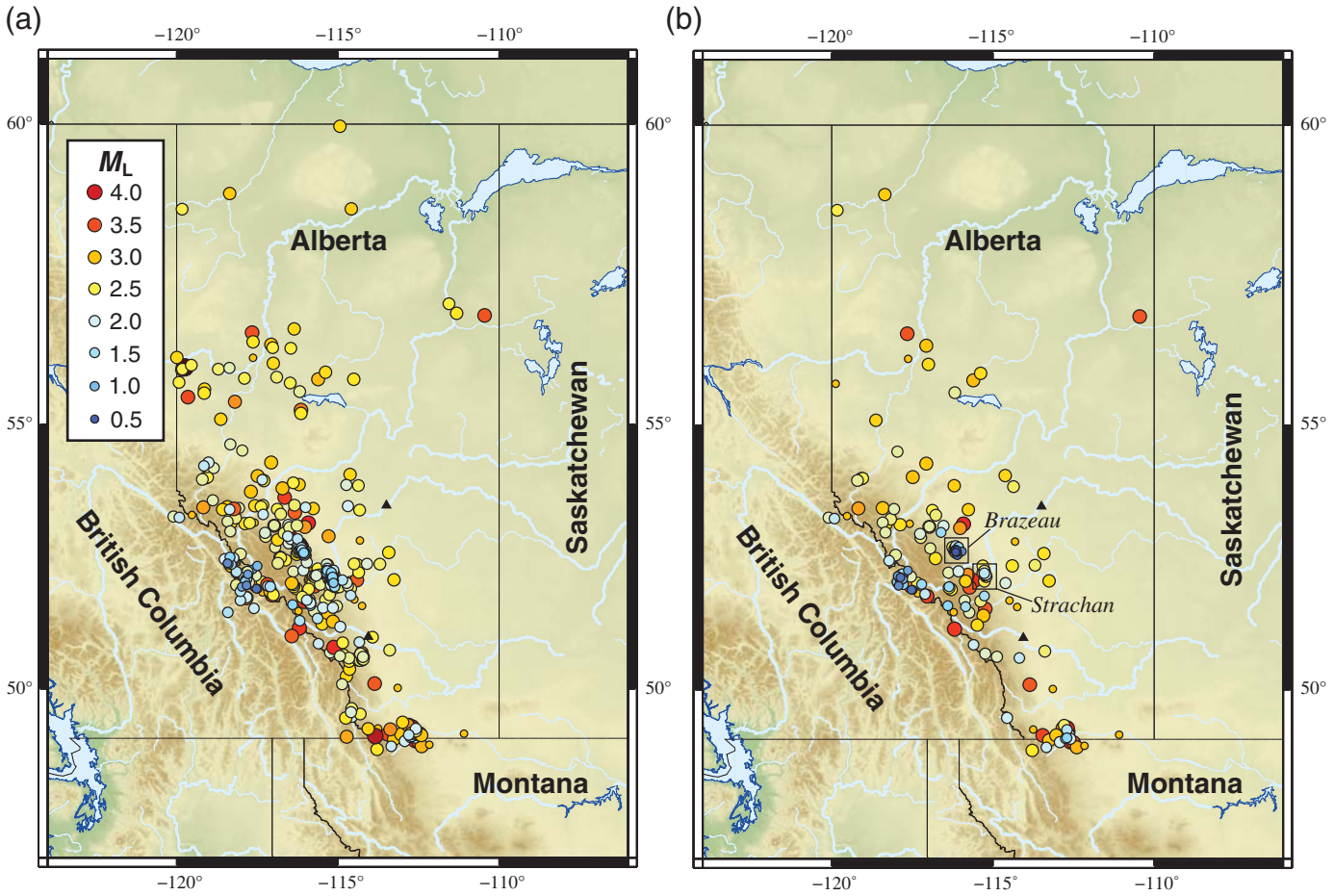

▲ **Figure 2.** (a) Distribution of seismicity in AB as recorded by all networks from September 2006 through 2010 and (b) for the Earthquakes Canada Catalogue (EqCC) from 1985 to September 2006. Event magnitudes are depicted by both size and shading according to the legend. Major cities are denoted by black triangles, and the Strachan and Brazeau River clusters are indicated by boxes on the second panel.

Analogously, high amplitude outliers in the higher frequency band (HB; <1 s) result from recordings of regional events, blasts, and teleseismic body waves; however, instrument self noise contributes little to the apparent high-amplitude, modal noise at these periods. Instead, cultural noise (McNamara and Buland, 2004) and wind intensity (Tsai *et al.*, 2012; Vassallo *et al.*, 2012) have been purported as the dominant effects at these periods. Naturally, cultural noise (e.g., Lombaert *et al.*, 2000; Coward *et al.*, 2003) will have a recurring daily, weekly, and even seasonal variations; for CRANE and ATSN these variations are likely the most pervasive source of noise, as most definitively observed at the station RW3 (Fig. 4). For example, an average day in 2010 nearby RW3 begins promptly at 6 a.m. and has a less stringent end time, with a peak variation in noise of 30 dB. Only at a handful of stations (e.g., CLA, PER, RW2, and RW4) is there limited, or the absence of, diurnal variations. Overall, recording stations are comparable, in HB noise levels, to similar deployments (Wilson *et al.*, 2002). Stations with an overall large noise amplitude in the HB are likely affected by defects during vault construction or site selection (Evangelidis and Melis, 2012) and will be recommended for future relocation.

EVALUATION OF NETWORK PERFORMANCE: MAGNITUDE OF COMPLETENESS

Understanding of the limitations of network performance is a critical step in gauging the quality of any earthquake catalog. Often, a measure of the M_c is used as a criterion to evaluate the performance of a seismic network (e.g., Mignan and Woessner, 2012). In other studies, M_c has been ascertained by determining the magnitude that departs (Wiemer and Wyss, 2000; Cao and Gao, 2002; Marsan, 2003; Woessner and Wiemer, 2005; Amorese, 2007) from the Gutenberg–Richter frequency–magnitude distribution (FMD, see Ishimoto and Iida, 1939; Gutenberg and Richter, 1942). Additional techniques to measure network performance are also available, which include the analysis of diurnal variations in network sensitivity (Rydelek and Sacks, 1989), seismic threshold monitoring (Gomberg, 1991; Kværna and Ringdahl, 1999; Kværna *et al.*, 2002), numerical simulation (D'Alessandro, Luzio, *et al.*, 2011; D'Alessandro, Papanastassiou, Baskoutas, 2011; D'Alessandro and Stickney, 2012), or Bayesian statistics (Mignan *et al.*, 2011; Kraft *et al.*, 2013; Mignan and Chouliaras, 2014). However,

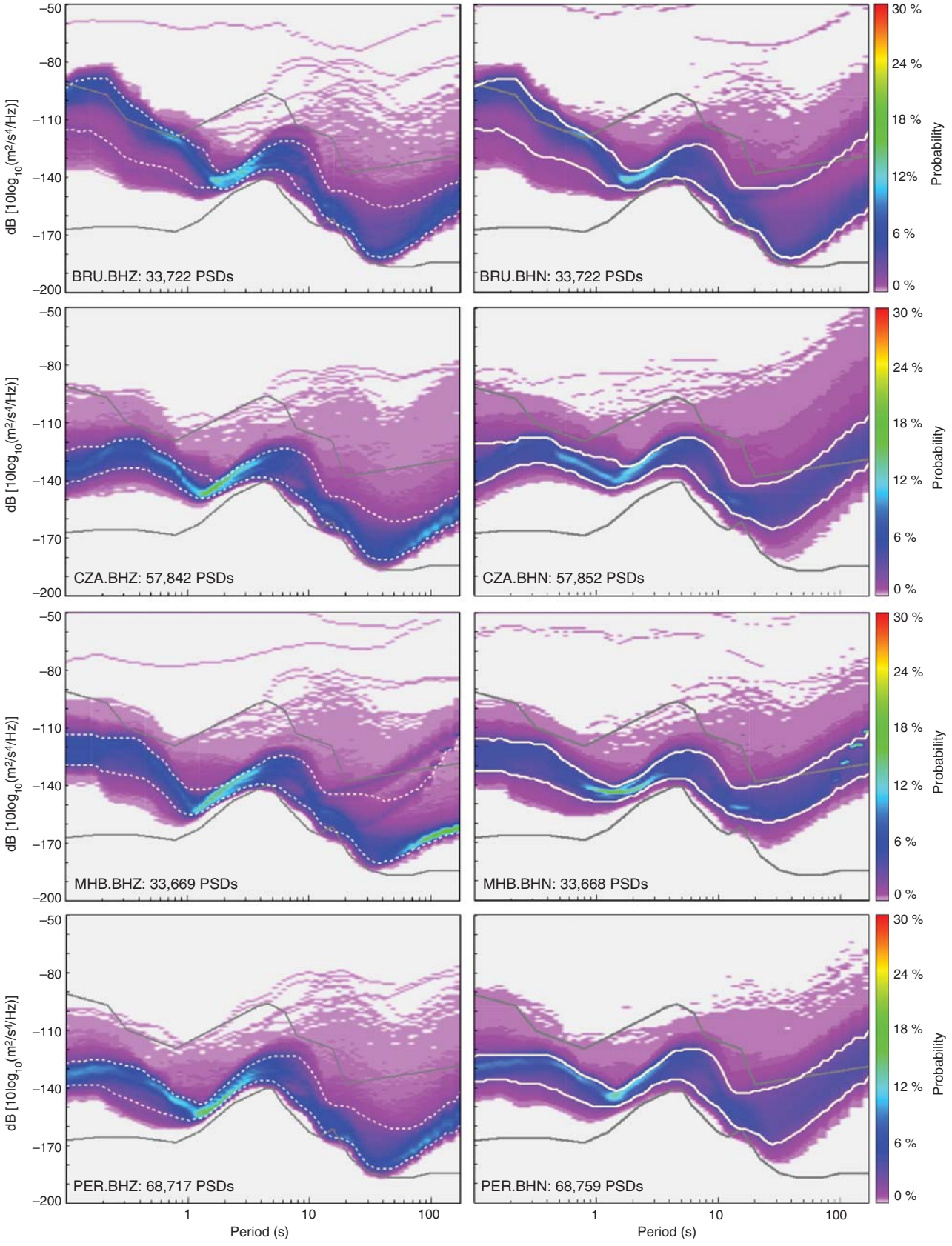

▲ **Figure 3.** PDFs constructed from continuous, vertical, and horizontal waveform data from CRANE waveforms. Noise is shown as a statistical distribution with first and last deciles shown (white lines). The new low-noise model (NLNM, lower dark line) and new high-noise model (NHNM, upper dark line) curves are shown for reference (Peterson, 1993).

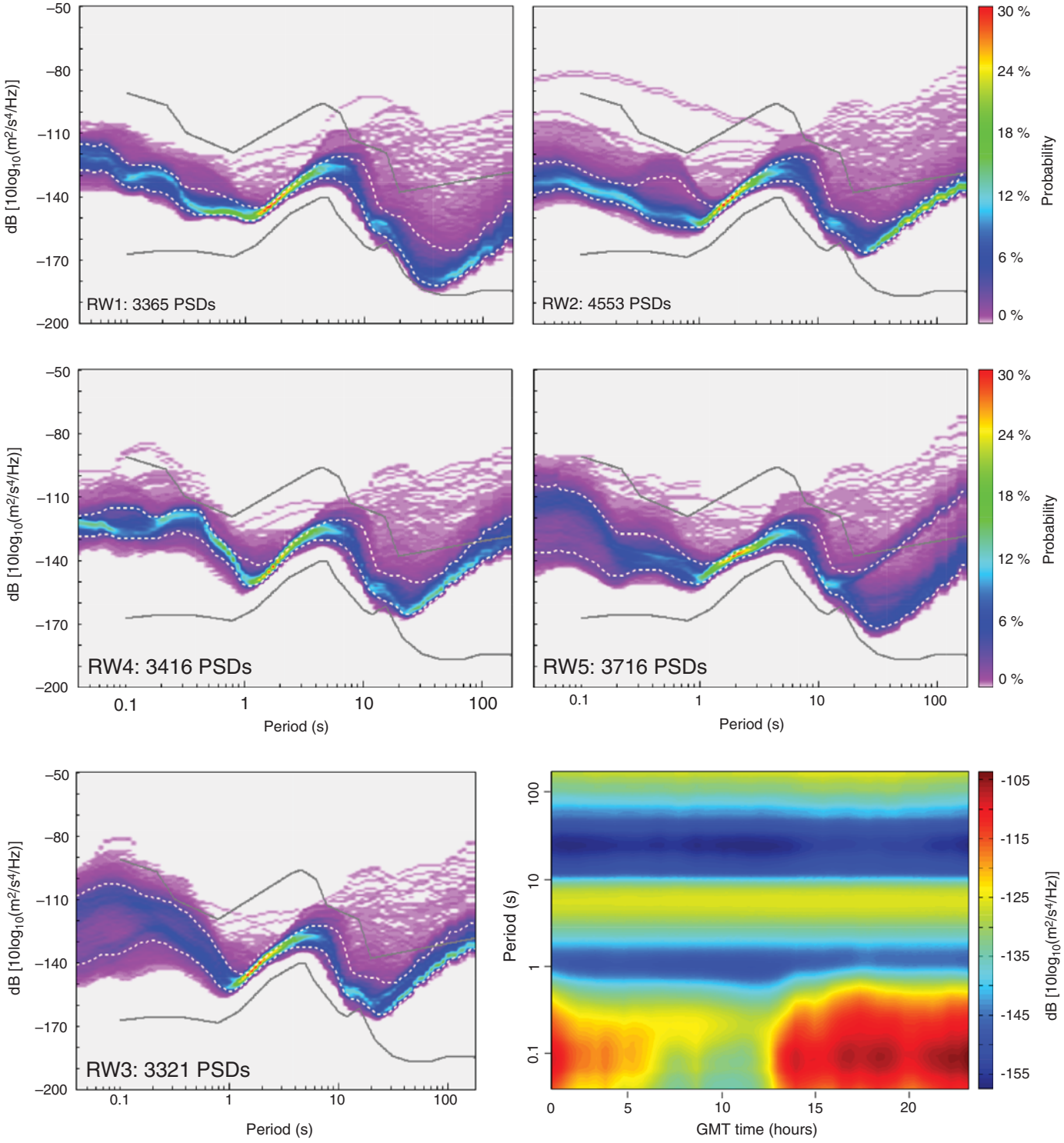

▲ **Figure 4.** Analogous plot to Figure 3 showing vertical component probability distribution functions of RWX deployments. The panel in the bottom right depicts the diurnal variation observed at station RW3 averaged over the 2010–2011 data, highlighting diurnal variability in noise at short periods.

the application of some of these techniques has been limited by the sparsity and quiescence in our catalog.

The relative quiescence of AB seismicity, in combination with historically sporadic receiver coverage, restricts the robust fitting of spatially or temporally modulated FMDs. Instead, we defer to synthetic tests to ascertain network performance spatially. In our context, M_c is defined as the minimum magnitude that allows for the robust detection, identification, and picking

of four P phases. We select a criteria of wideband spectral ratio (WSR) greater than 10.0 to ensure that phase pick errors would be unaffected by noise (Zeiler and Velasco, 2009). WSR is defined by the expression

$$\mathrm{WSR} = \frac{\sqrt{P_S}}{\sqrt{P_N}}. \tag{1}$$

To achieve this measure as a function of source distance and earthquake magnitude, we further investigate relationships of the numerator (power of signal P_S) and the denominator (power of noise P_N) terms.

Our estimation of the signal portion P_S follows the methods described in D'Alessandro, Luzio, *et al.* (2011). The envelope of the azimuthally averaged earthquake spectrum $\bar{S}_s(r, \omega)$ is defined by the formula (Aki and Richards, 2002)

$$\bar{S}_s(r, \omega) = \frac{C_S M_0}{1 + (\omega/\omega_0)^2} \omega^n, \tag{2}$$

in which M_0 is defined as the seismic moment, ω_0 is the corner frequency, and n is an integer responsible for indicating displacement (0), velocity (1), or acceleration (2) spectra. The circular fault model of Brune (1970) accurately describes the near- and far-field spectra of earthquakes via the consideration of the effective stress drop along the sides of a fault. For our purposes, this circular fault model defines the far-field amplitude C_S while assuming homogenous, elastic media. Effects of geometrical spreading are included in this formulation through its inverse dependence on hypocentral distance r (see D'Alessandro, Luzio, *et al.*, 2011 for details). The explicit dependence on stress drop $\Delta\sigma$ is apparent in the formulation of cutoff frequency as

$$\omega_0 = \left(\frac{16\Delta\sigma}{7M_0 k}\right)^{1/3} c. \tag{3}$$

In our study, a stress drop of 6 MPa (60 bar) was selected based on results from studies on earthquake source parameters in AB (e.g., Rebollar *et al.*, 1982, 1984). The additional term k is a constant dependent on the rupture velocity (3.36 for P waves and 2.34 for S waves), and c is the seismic velocity of the medium. For convenience, the seismic scalar moment has been mapped to local magnitudes M_L via the relationship of Hanks and Kanamori (1979), which is applicable for moderately sized earthquakes. Although our choices for input parameters are reflective of the earthquakes in AB, we do note the potential for variability in their values. For example, to account for some of this variability we perturb the input stress range (1–10 MPa) in our method. Overall, we expect that our synthetic constraints on M_c can range from +0.35 to −0.15 as compared to empirical observation.

The spectrum of an earthquake $\bar{S}_s(\omega)$ is readily calculated for all relevant P phases (Pg, Pn, and PmP) given a hypocentral distance and M_L. The details of equation (2), coupled with the model of Brune (1970), consider elastic attenuation (geometrical spreading) factors for homogenous media. However, anelastic attenuation factors (e.g., scattering and intrinsic attenuation) have a considerable effect on the resultant spectrum

$$\bar{S}(r, \omega) = \bar{S}_s(r, \omega) A(r, \omega), \tag{4}$$

in which the properties of anelastic attenuation $A(r, \omega)$ are defined through the exponential loss relationship

$$A(r, \omega) = \exp\left(\frac{-\omega r}{2cQ(\omega)}\right), \tag{5}$$

which is based on the media dependent attenuation quality factor $Q(\omega)$. In this study, we use the empirically derived attenuation curves of Atkinson (2004). To verify the applicability of this model, we estimated the quality factor Q regional to AB using a simplified reversed two-station method (see Zhu *et al.*, 1991). Values from this analysis ($\sim 2 \times 10^3$) as well as prior studies (Clowes and Kanasewich, 1970) suggest that the adopted model (Atkinson, 2004) remains approximately applicable to phase attenuation in AB.

Finally, the power of the signal is proportional to the average of the squared spectral magnitude

$$P_S = \left(\frac{1}{\omega_b - \omega_a}\right) \int_{\omega_a}^{\omega_b} |\bar{S}(r, \omega)|^2 d\omega. \tag{6}$$

Integration is restricted to a range $(\omega_a - \omega_b)$ of relevant frequencies to ensure the fidelity of our results; the lower ($2\pi \times 1$ Hz) filters unwanted, long-period noise irrelevant to regional seismicity, while the upper bound stops before the onset of instrument anti-aliasing filters (~60% of the Nyquist frequency). Analogously, the power of noise was calculated based on the modal values of noise estimated from the PDFs discussed previously.

To investigate the spatial performance of the network, earthquakes of varying magnitude were simulated on a regular grid of approximately 5×5 km^2 and fixed at a depth of 5 km. The magnitude threshold map (Fig. 5) quantifies the time-averaged spatial extent of the composite network and CNSN performance. CNSN alone has thresholds approaching a magnitude of 2.25–2.50 for the central AB Rockies and foothills; however, the limitations of sparser station coverage become apparent ($M_\mathrm{L} > 3.0$) in the extremities, especially the northeastern corner. Circular regions of substantially increased detectability around stations (visible for DOWB, MNB, BLBC, and SLEB) at ~100 km radius are due to the onset of Pn arrivals, which geometrically spread more slowly than does Pg. The addition of CRANE, ATSN, and MRSN greatly improves and extends detection thresholds (Fig. 5). PRDA and MRSN stations play a key role in improving performance ($M_\mathrm{L} < 2.0$) in southern AB. CRANE stations, in particular PER and NOR, remove the saddle shape in detection thresholds near the Strachan and Brazeau clusters and reduce the M_c in these regions to as low as ~2.0. CRANE Redwater deployments are also largely responsible for extending the coverage into central AB.

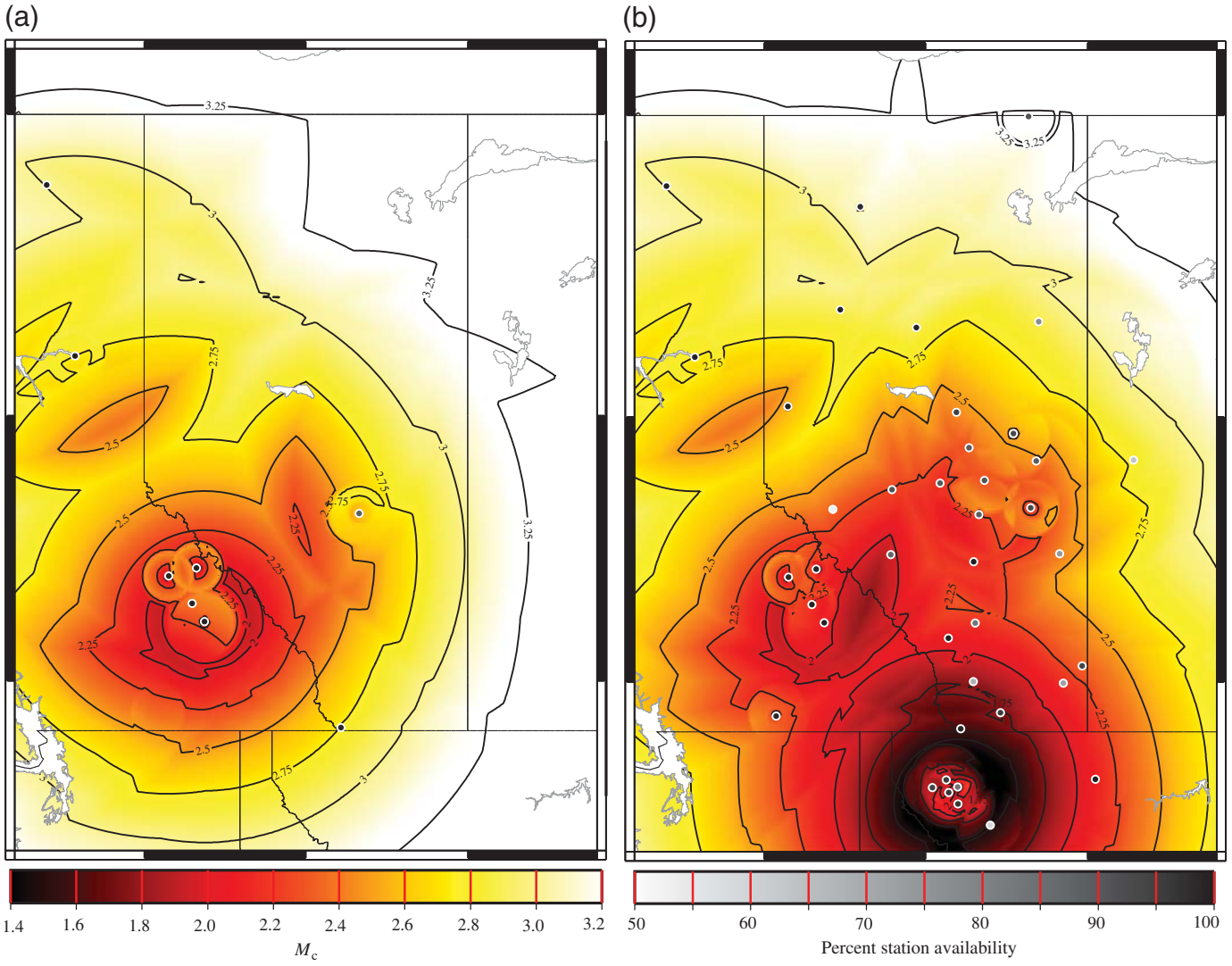

▲ **Figure 5.** Estimated magnitude of completeness for stations during 2010 based on a synthetic model. Thresholds calculated as the minimum magnitude permitting reliable *P*-phase picks on at least four stations. (a) CNSN stations operational during 2010, whereas (b) is the composite performance of all operational stations used in the compilation of the Alberta Geological Survey earthquake catalogue. Available stations are depicted as circles, colored according to their data availability (b). The large bulk of stations are available for the majority of time (90 + %); however, a few stations do have data gaps, or transient outages in excess of this.

Lastly, the spatial dependence of M_c is examined through the empirical relationship

$$M_c(r,k) = C_1 r^{C_2} + C_3, \tag{7}$$

which is dependent on distance r to the kth nearest station with fit parameters C_1, C_2, and C_3 (Mignan *et al.*, 2011). Our simulated M_c map is fit to this empirical relationship via a linear regression of the data with a fixed C_3 value; this process is repeated for perturbed C_3 values and the one that minimizes the variance of the residuals is chosen as optimal. We find the best fit to the data with $C_1 = 7.66$, $C_2 = 0.0663$, $C_3 = -8.83$, $k = 4$, and a standard deviation of the residuals of 0.28 (Fig. 6). This fit to our synthetic data is comparable to catalog derived fits in other regions such as Taiwan (Mignan *et al.*, 2011), Greece (Mignan and Chouliaras, 2014), and Switzerland (Kraft *et al.*, 2013). Overall, this empirical $M_c(r)$ function could be instructive for any agencies considering future site installations in the WCSB.

PERFORMANCE OF CATALOGED SEISMICITY

During the study period more than 3500 events were located in the WCSB and the Rockies (Stern *et al.*, 2013), the vast majority of which can be attributed to nontectonic sources, that is, quarry blasts and other artificial explosions. We categorized seismicity as nontectonic based on (1) the timing of the event (e.g., blasting occurs during daylight hours), (2) the proximity

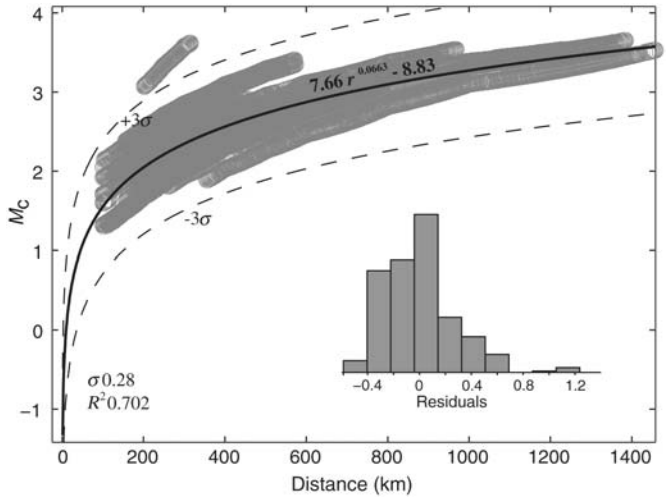

▲ **Figure 6.** Fit of M_c versus distance to the 4th nearest station (gray circles) to an empirical function (solid black line) with error bounds of $\pm 3\sigma$ (dashed lines). Inset depicts a histogram of the M_c residuals to the function fit.

of the event to nearby sources, such as quarries, and finally, (3) characteristics of the waveform; blasts have certain waveform distinctions (e.g., predominantly compressional first motions, and high-frequency, monochromatic spectral content) that may distinguish them from earthquakes (e.g., Dahy and Hassib, 2010). To limit the number of blasts misidentified as earthquakes, our catalog was inspected based on a spatial averaging (~250 × 250 km^2 bins) of the ratio between daytime and nighttime events (e.g., Wiemer and Baer, 2000; Wiemer, 2001). The ratios are perturbed closely to unity (~0.9), suggesting there is minimal earthquake-explosion misidentification. More than 170 magnitude (M_L) 0.4–4.1 events remain after the removal of nontectonic events (Fig. 2), which almost doubles the number of reported regional earthquakes during the same period in the EqCC.

As previously mentioned, the sparsity and quiescence of earthquakes in the WCSB limits the practicality of empirically determining our catalog's performance spatially or temporally. However, regions of clustered and background seismicity contain sufficient data to establish performance measurements for rudimentary comparison to our synthetic results. In this section, we determine the M_c for the Strachan (Wetmiller, 1986), Brazeau (Schultz *et al.*, 2014), and declustered WCSB background seismicity. To do so, we amalgamate data from the EqCC (January 1985 to September 2006) with the AGS catalog, and the regional background seismicity is declustered via the algorithm of Reasenberg (1985), a routine included in the catalog analysis package ZMAP (Wiemer, 2001). Figure 7 shows the maximum-likelihood estimates of seismic *b*-values (Aki, 1965; Marzocchi and Sandri, 2003) and its uncertainty (Shi and Bolt, 1982) computed for subsets of the earthquake catalog as well as the combination with the EqCC. In view that a poor choice of M_c can cause a bias in the determination of seismic *b*-value, we estimate *b*-values based on an M_c that maximizes the goodness of fit to the data (e.g., Wiemer and Wyss, 2000). Both the Strachan and Brazeau data fit the FMD well, showing M_cs of 1.94 and 2.24 as well as *b*-values of 0.743 ± 0.059 and 0.999 ± 0.139 (Fig. 7b,c), respectively. These empirically determined values are comparable to our synthetically computed threshold values of $M_L \sim 2.0$ for both clusters.

Results from background declustered catalog (Fig. 7a) indicate that an optimal M_c of 2.45 and a seismic *b*-value of 1.020 ± 0.084 best fit the data regionally. Examination of the *b*-value (see Fig. 7) shows that the goodness of fit to the background catalog FMD is poorer in comparison with the clustered data (e.g., R^2 values of 0.820 versus 0.992). This is likely attributable to the spatial performance of the network; in Figure 5 we see that detection thresholds, in relevant areas, are largely controlled by a few select stations (BLBC, MNB, SLEB, and DOWB) with M_c thresholds diminishing circularly from them. Because the background catalog is sampling a spatial region with a high degree of variability in M_c (< 2.0–3.0+) there is no longer a sharp M_c cutoff observed in the FMD. Interestingly, the recent subset of the background catalog (symbolized as + in Fig. 7) exhibits a sharp cutoff at ~2.25 and a kink in the cumulative FMD at 2.75. This is consistent with the changes in network capacity revealed by simulation because (1) with the exception of a few northern events, the vast majority of seismicity is encapsulated by the simulated 2.75 contours (see Figs. 5 and 2), and (2) network performance has greatly increased in the central Rockies (see the changes in contour lines for M_c 2.25). This feature may be an artifact associated with temporally and spatially changing network setup and station density. In fact, a statistical times-series analysis of the long-term average (Matthews and Reasenberg, 1988; Reasenberg and Simpson, 1992; Wiemer, 2001) of background events (truncated at $M_L > 2.5$) reveals that the most statistically significant changes in the rate of documented seismicity were increases during September 2006 (3σ confidence) and the beginning of 2010 ($> 5\sigma$ confidence). These two points in time coincide with the initiation of the new catalog (September 2006) as well as the rapid deployment of several stations (RWX, RDR, RAYA) relevant to seismically active areas.

EVALUATION OF NETWORK RESOLUTION: EPICENTER VARIANCE

The value of M_c is a useful measure of a network's ability to detect events, but it contains limited information about the validity of event locations. As a counterpart to the M_c criterion, we assess the spatial resolution of location variance by evaluating the covariance matrix of the solution $\mathbf{C_h}$:

$$\mathbf{C_h} = (\mathbf{G}^T \mathbf{C}_d^{-1} \mathbf{G})^{-1}. \quad (8)$$

The matrix $\mathbf{G}$ is constructed from the partial derivatives of the travel-time function with respect to each event coordinate. Travel-time functions are generated for our velocity model us-

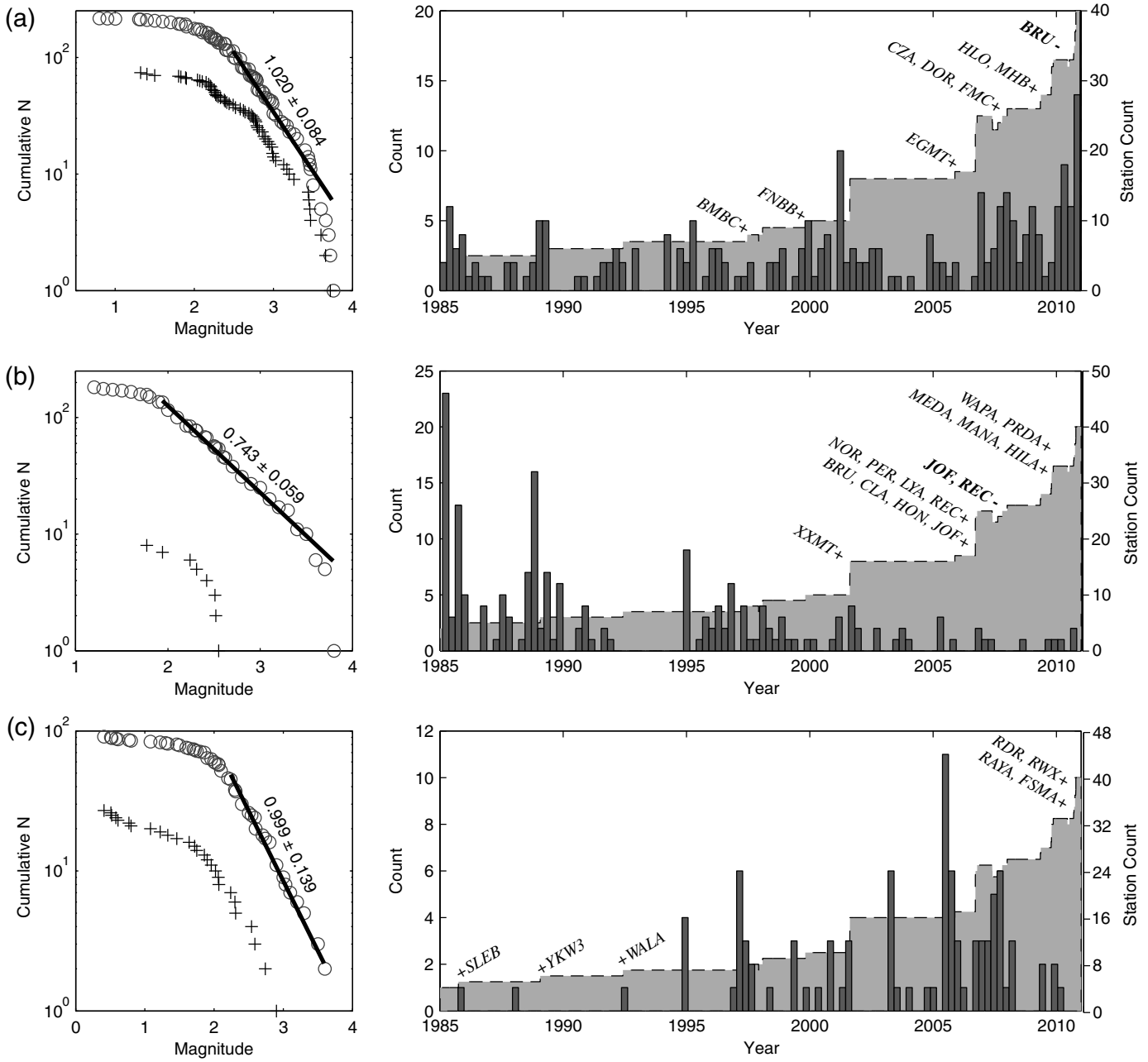

▲ **Figure 7.** The earthquake catalogs are analyzed in subsets: (a) the regional catalog, (b) the Strachan cluster, and (c) the Brazeau cluster. Frequency–magnitude distributions are depicted (left side) for all subsets of data. This study's catalog data (crosses) and the composite with EqCC data (circles) have been best fitted (dark line) with *b*-values. Histograms of the temporal variation in earthquake distribution (bars) are depicted on the right side. As well, the availability of stations is superimposed (gray-filled dashed line) with annotations of station changes. The stations PNT, EDM, MNB, and DOWB were already operational at the onset of 1985.

ing TauP (Crotwell *et al.*, 1999). Given a hypothetical source location, our **G** matrix is populated with first arriving phase from both *P* and *S* for each station meeting the prior criteria of a WSR > 10. The matrix $\mathbf{C_d}$ is assumed to be a diagonal matrix representing the covariance of the data, which are based on the inverse of the standard variance of phase picks. Our standard errors of 0.21 s, 0.21 s, 0.41 s, and 0.49 s for the respective phase picks of *Pg*, *Pn*, *Sg*, and *Sn* are estimated from the catalog residuals of more than 3500 events. The covariance matrix of the solution $\mathbf{C_h}$ represents the standard error ellipsoid. It is important to note, however, that this ellipsoid encompasses only the minimization of standard error in hypocenter location and does not reflect additional errors/biases introduced by a local minimum solution, a systematically incorrect velocity model or the presence of crustal anisotropy/heterogeneity (e.g., Flanagan *et al.*, 2007).

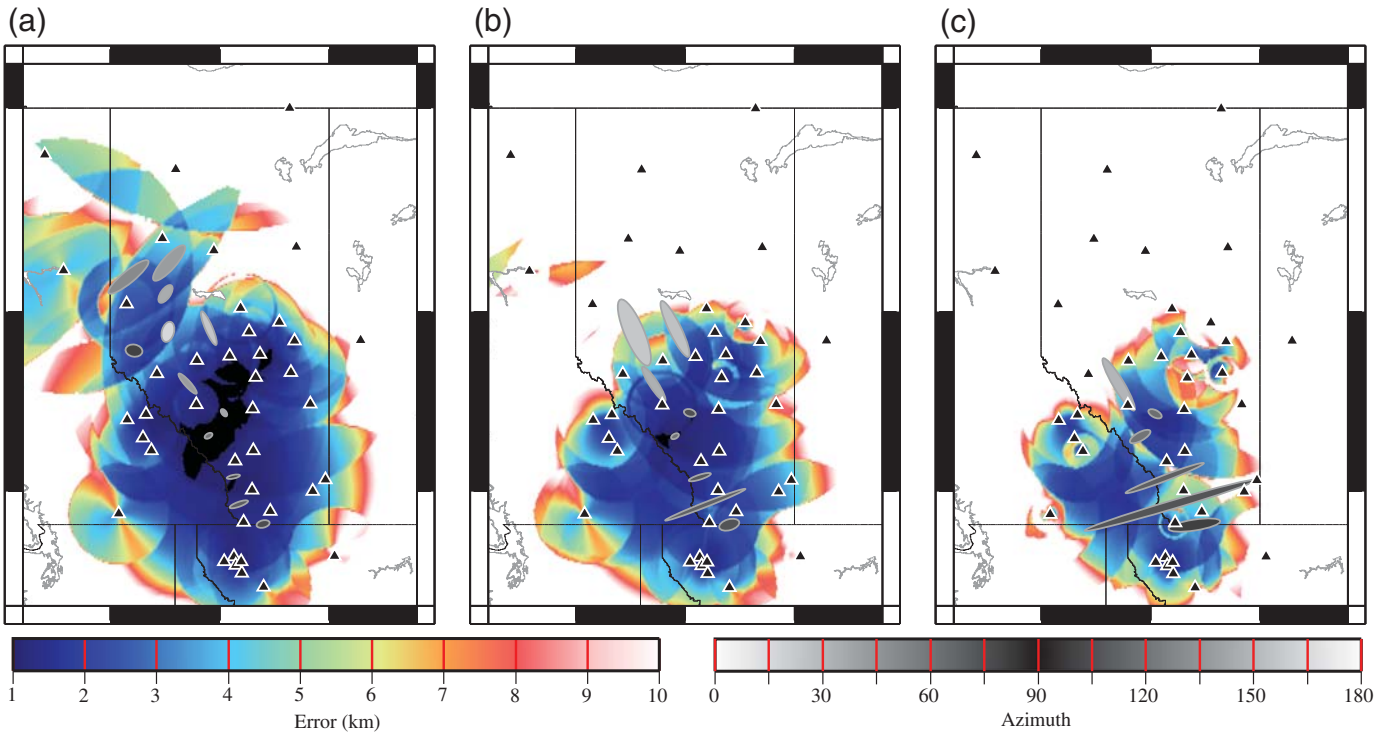

▲ **Figure 8.** Variations in the standard error of epicentral locations. Epicentral error accommodates both semimajor and semiminor axes of the error ellipse in a geometric mean as the equivalent circular radius. Maps are based on the hypothetical signal from magnitude 3.0, 2.75, and 2.5 Brune source (a, b, and c, respectively). In addition, error ellipsoids are superimposed at various locations to depict scaling between semimajor and semiminor axes and azimuths. Relevant stations are depicted as triangles.

Standard error maps (Fig. 8) are constructed based on the 95% confidence interval and identical spatial sampling as the M_c maps (5×5 km^2). The standard error ellipsoid is reduced to an epicentral error by a geometrical average of the semimajor and semiminor axis radii to an equivalent circular radius. All stations in operation during 2010 are considered in our simulation of magnitude 3.0, 2.75, and 2.5 earthquakes. Epicentral error maps show circular features with major drop off after a critical distance; these drop-offs in resolution are an artifact of suddenly turning off stations that are unable to meet the WSR $>$ 10 criterion. Stations with WSR $<$ 10 could be incorporated into these maps by further analyzing the statistics of phase pick errors versus WSR/distance. Figure 8 shows an excellent (~1 km) epicentral resolution in well sampled areas south of 55° N for all simulated earthquake magnitudes. Locations in northern AB about WAPA for larger earthquakes (M_L 3.0) are most poorly constrained (~5 km error) due to the sparsity of stations in this region. Further simulations with smaller magnitude earthquakes (M_L 2.75) display significant reductions in resolution in northern AB near WAPA (tens of kilometers), with more modest reductions to ~5 km on the fringe of the recording networks. The final simulation of M_L 2.5 events reveals a complete loss of resolution in the vicinity of WAPA, which has been previously evidenced by the difficulty of locating smaller blasts from mining operations in the region (Stern *et al.*, 2013). Magnitude 2.5 earthquakes are best constrained (1–2 km) along the Rocky Mountains and into southern AB with gaps emerging intermittently in central AB.

CONCLUSIONS

The addition of CRANE, ATSN, and MRSN networks has greatly benefitted the understanding of seismicity in the Rocky Mountains and the WCSB. Noise analysis of seismic data constrains station performance providing insight to the nature of noise encountered on an hour-to-hour basis. The AGS regional earthquake catalog is the most comprehensive to date in AB, a region previously undersampled by seismic instruments, and our integrated analyses based on body-wave earthquake location, systematic noise characterization, and standard error maps begin to quantify this improvement. More exhaustive attempts at cataloging AB seismicity would benefit from increased station density, with threshold and standard error maps prioritizing locations of future deployments. Results from this study suggest that increased station density is best directed in areas of poorer detection thresholds and epicenter resolution, such as northern AB near WAPA and southern AB.

DATA AND RESOURCES

Seismic waveform data used in this paper originated from multiple sources including the Canadian Rockies and Alberta Network, which is operated by the University of Alberta, the

Canadian National Seismic Network, which is operated by the Geological Survey of Canada (Earthquakes Canada, 2013a), the Alberta Telemetered Seismic Network, which is operated by the University of Calgary, the Montana Regional Seismic Network, which is operated by the Montana Bureau of Mines and Geology, and finally USArray, which is operated by the United States Geological Survey. The catalog of prior seismicity in AB (1985–September 2006) was acquired through an online download from the Natural Resources Canada website (Earthquakes Canada, 2013b). The catalog of recent seismicity used in this study is available through the AGS website (Stern *et al.*, 2013). Hypocenter inversions were performed using the seismic software Antelope from Boulder Real Time Technologies Inc., noise analysis used the software PQLX (McNamara and Buland, 2004; McNamara and Boaz, 2011), and portions of earthquake catalog analysis used ZMAP (Wiemer, 2001). Maps were made using Generic Mapping Tools (Wessel and Smith, 1998).

ACKNOWLEDGMENTS

We would like to thank Honn Kao and an anonymous reviewer for their suggestions in the preparation of this paper. The University of Alberta would like to thank the Canadian Foundation for Innovation (CFI) and all the host families of the seismomic instruments for their generous support.

REFERENCES

Aki, K. (1965). Maximum likelihood estimate of b in the formula $\log(N) = a - b\mathrm{M}$ and its confidence limits, *Bull. Earthq. Res. Inst. Tokyo Univ.* **43,** 237–239.

Aki, K., and P. G. Richards (2002). *Quantitative Seismology: Theory and Methods*, University Science Books, Sausalito, California.

Amorese, D. (2007). Applying a change-point detection method on frequency-magnitude distributions, *Bull. Seismol. Soc. Am.* **97,** 1742–1749, doi: 10.1785/0120060181.

Atkinson, G. M. (2004). Empirical attenuation of ground-motion spectral amplitudes in southeastern Canada and the northeastern United States, *Bull. Seismol. Soc. Am.* **94,** 1079–1095, doi: 10.1785/0120030175.

Baranova, V., A. Mustaqeem, and S. Bell (1999). A model for induced seismicity caused by hydrocarbon production in the Western Canada Sedimentary Basin, *Can. J. Earth Sci.* **36,** no. 1, 47–64, doi: 10.1139/e98-080.

BC Oil and Gas Commission (2012). Investigation of observed seismicity in the Horn River Basin, 29 pp., http://www.bcogc.ca/node/8046/download (last accessed December 2013).

Beauduin, P., P. Lognonne, J. Montagner, S. Cacho, J. Karczewski, and M. Morand (1996). The effects of atmospheric pressure changes on seismic signals, or how to improve the quality of a station, *Bull. Seismol. Soc. Am.* **86,** 1760–1799.

Brune, J. N. (1970). Tectonic stress and the spectra of seismic shear waves from earthquakes, *J. Geophys. Res.* **75,** 4997–5009, doi: 10.1029/JB075i026p04997.

Burtin, A., L. Bollinger, J. Vergne, R. Cattin, and J. L. Nabelek (2008). Spectral analysis of seismic noise induced by rivers: A new tool to monitor spatiotemporal changes in stream hydrodynamics, *J. Geophys. Res.* **113,** no. B05301, doi: 10.1029/2007JB005034.

Burtin, A., J. Vergne, L. Rivera, and P. Dubernet (2010). Location of river-induced seismic signal from noise correlation functions, *Geophys. J. Int.* **182,** 1161–1173, doi: 10.1111/j.1365-246X.2010.04701.x.

Cao, A. M., and S. S. Gao (2002). Temporal variations of seismic b-values beneath northeastern Japan island arc, *Geophys. Res. Lett.* **29,** 48-1–48-3, doi: 10.1029/2001GL013775.

Clowes, R. M., and E. R. Kanasewich (1970). Seismic attenuation and the nature of reflecting horizons within the crust, *J. Geophys. Res.* **75,** 6693–6705, doi: 10.1029/JB075i032p06693.

Coward, D., D. Blair, R. Burman, and C. Zhao (2003). Vehicle-induced seismic effects at a gravitational wave observatory, *Rev. Sci. Instrum.* **74,** 4846–4854, doi: 10.1063/1.1614411.

Crotwell, H. P., T. J. Owens, and J. Ritsema (1999). The TauP Toolkit: Flexible seismic travel-time and ray-path utilities, *Seismol. Res. Lett.* **70,** 154–160, doi: 10.1785/gssrl.70.2.154.

Dahy, S. A., and G. H. Hassib (2010). Spectral discrimination between quarry blasts and microearthquakes in southern Egypt, *Res. J. Earth Sci.* **2,** 1–7.

D'Alessandro, A., and M. Stickney (2012). Montana seismic network performance: An evaluation through the SNES method, *Bull. Seismol. Soc. Am.* **102,** no. 1, 73–87, doi: 10.1785/0120100234.

D'Alessandro, A., D. Luzio, G. D'Anna, and G. Mangano (2011). Seismic network evaluation through simulation: An application to the Italian National Seismic Network, *Bull. Seismol. Soc. Am.* **101,** no. 3, 1213–1232, doi: 10.1785/0120100066.

D'Alessandro, A., D. Papanastassiou, and I. Baskoutas (2011). Hellenic Unified Seismological Network: An evaluation of its performance through SNES method, *Geophys. J. Int.* **185,** 1417–1430, doi: 10.1111/j.1365-246X.2011.05018.x.

De Angelis, S., and P. Bodin (2012). Watching the wind: Seismic data contamination at long periods due to atmospheric pressure-field-induced tilting, *Bull. Seismol. Soc. Am.* **102,** 1255–1265, doi: 10.1785/0120110186.

Diaz, J., A. Villasenor, J. Morales, A. Pazos, D. Cordoba, J. Pulgar, J. L. Garcia-Lobon, M. Harnafi, R. Carbonell, J. Gallart, and TopoIberia Seismic Working Group (2010). Background noise characteristics at the IberArray Broadband Seismic Network, *Bull. Seismol. Soc. Am.* **100,** no. 2, 618–628, doi: 10.1785/0120090085.

Earthquakes Canada (2013a). GSC, Earthquake Search Continuous Waveform Archive, Pacific Geoscience Centre.

Earthquakes Canada (2013b). GSC, Earthquake Search (Online Bulletin), *Nat. Res. Can.* http://earthquakescanada.nrcan.gc.ca/stndon/NEDB-BNDS/bull-eng.php.

Eaton, D. (2014). Alberta Telemetered Seismograph Network (ATSN): Real-time monitoring of seismicity in northern Alberta, *CSEG Recorder* **39,** no. 3, 30–33.

Ellis, R. M., and B. Chandra (1981). Seismicity in the Mica Reservoir (McNaughton Lake) area: 1973–1978, *Can. J. Earth Sci.* **18,** 1708–1716, doi: 10.1139/e81-157.

Evangelidis, C. P., and N. S. Melis (2012). Ambient noise levels in Greece as recorded at the hellenic unified seismic network, *Bull. Seismol. Soc. Am.* **102,** 2507–2517, doi: 10.1785/0120110319.

Farahbod, A. M., H. Kao, D. M. Walker, and J. F. Cassidy (2014). Investigation of regional seismicity before and after hydraulic fracturing in the Horn River Basin, northeast British Columbia, *Can. J. Earth Sci.*, doi: 10.1139/cjes-2014-0162.

Flanagan, M. P., S. C. Myers, and K. D. Koper (2007). Regional travel-time uncertainty and seismic location improvement using a three-dimensional a priori velocity model, *Bull. Seismol. Soc. Am.* **97,** 804–825, doi: 10.1785/0120060079.

Gomberg, J. (1991). Seismicity and detection/location threshold in the southern Great Basin seismic network, *J. Geophys. Res.* **96,** no. B10, 16401–16414, doi: 10.1029/91JB01593.

Gu, Y. J., and L. Shen (2012). Microseismic noise from large ice-covered lakes? *Bull. Seismol. Soc. Am.* **102,** 1155–1166, doi: 10.1785/0120100010.

Gu, Y. J., A. Okeler, L. Shen, and S. Contenti (2011). The Canadian rockies and Alberta network (CRANE): New constraints on the

Rockies and Western Canada sedimentary basin, *Seismol. Res. Lett.* **82,** 575–588, doi: 10.1785/gssrl.82.4.575.
Gutenberg, B., and C. F. Richter (1942). Earthquake magnitude, intensity, energy, and acceleration, *Bull. Seismol. Soc. Am.* **32,** 163–191.
Hanks, T. C., and H. Kanamori (1979). A moment magnitude scale, *J. Geophys. Res.* **84,** 2348–2350.
Hasselmann, K. (1963). A statistical analysis of the generation of microseisms, *Rev. Geophys.* **1,** 177–209, doi: 10.1029/RG001i002p00177.
Horner, R. B., J. E. Barclay, and J. M. MacRae (1994). Earthquakes and hydrocarbon production in the Fort St. John area of northeastern British Columbia, *Can. J. Explor. Geophys.* **30,** 39–50.
Ishimoto, M., and K. Iida (1939). Observations of earthquakes registered with the microseismograph constructed recently, *Bull. Earthq. Res. Inst.* **17,** 443–478.
Koper, K. D., B. de Foy, and H. M. Benz (2009). Composition and variation of noise recorded at the Yellowknife Seismic Array, 1991–2007, *J. Geophys. Res.* **114,** no. B10310, doi: 10.1029/2009JB006307.
Kraft, T., A. Mignan, and D. Giardini (2013). Optimization of a large-scale microseismic monitoring network in northern Switzerland, *Geophys. J. Int.* **195,** 474–490, doi: 10.1093/gji/ggt225.
Kværna, T., and F. Ringdal (1999). Seismic threshold monitoring for continuous assessment of global detection capability, *Bull. Seismol. Soc. Am.* **89,** no. 4, 946–959.
Kværna, T., F. Ringdahl, J. Schweitzer, and L. Taylor (2002). Optimized seismic threshold monitoring-part 1: Regional processing, *Pure Appl. Geophys.* **159,** no. 5, 969–987, doi: 10.1007/s00024-002-8668-0.
Lombaert, G., G. Degrande, and D. Clouteau (2000). Numerical modeling of free field traffic-induced vibrations, *Soil Dynam. Earthq. Eng.* **19,** 473–488, doi: 10.1016/S0267-7261(00)00024-5.
Longuet-Higgens, M. S. (1950). A theory of the origin of microseisms, *Phil. Trans. Roy. Soc. Lond.* **243,** 1–35, doi: 10.1098/rsta.1950.0012.
Marsan, D. (2003). Triggering of seismicity at short timescales following California earthquakes, *J. Geophys. Res.* **108,** no. B5, 2266, doi: 10.1029/2002JB001946.
Marzocchi, W., and L. Sandri (2003). A review and new insights on the estimation of the *b*-value and its uncertainty, *Ann. Geophys.* **46,** 1271–1282.
Matthews, M. V., and P. A. Reasenberg (1988). Statistical methods for investigating quiescence and other temporal seismicity patterns, *Pure Appl. Geophys.* **126,** 357–372, doi: 10.1007/BF00879003.
McNamara, D. E., and R. I. Boaz (2011). PQLX: A seismic data quality control system description, applications, and users manual, *U.S. Geol. Surv. Open-File Rept. 2010-1292*, 41.
McNamara, D. E., and R. P. Buland (2004). Ambient noise levels in the continental United States, *Bull. Seismol. Soc. Am.* **94,** 1517–1527, doi: 10.1785/012003001.
Mignan, A., and G. Chouliaras (2014). Fifty years of seismic network performance in Greece (1964–2013): Spatiotemporal evolution of the completeness magnitude, *Seismol. Res. Lett.* **85,** no. 3, 657–667, doi: 10.1785/0220130209.
Mignan, A., and J. Woessner (2012). Estimating the magnitude of completeness for earthquake catalogs, *Community Online Resource for Statistical Seismicity Analysis*, doi: 10.5078/corssa-00180805.
Mignan, A., M. J. Werner, S. Wiemer, C. C. Chen, and Y. M. Wu (2011). Bayesian estimation of the spatially varying completeness magnitude of earthquake catalogs, *Bull. Seismol. Soc. Am.* **101,** no. 3, 1371–1385, doi: 10.1785/0120100223.
Milne, W. G. (1970). The Snipe Lake, Alberta earthquake of March 8, 1970, *Can. J. Earth Sci.* **7,** 1564–1567, doi: 10.1139/e70-148.
Peterson, J. (1993). Observation and modeling of seismic background noise, *U. S. Geol. Surv. Technical Rept. 93-322*, 1–95.
Reasenberg, P. A. (1985). Second-order moment of central California seismicity, 1969–1982, *J. Geophys. Res.* **90,** 479–495, doi: 10.1029/JB090iB07p05479.
Reasenberg, P. A., and R. W. Simpson (1992). Response of regional seismicity to the static stress change produced by the Loam Prieta earthquake, *Science* **255,** 1687–1690, doi: 10.1126/science.255.5052.1687.
Rebollar, C. J., E. R. Kanasewich, and E. Nyland (1982). Source parameters from shallow events in the Rocky Mountain House earthquake swarm, *Can. J. Earth Sci.* **19,** 907–918, doi: 10.1139/e82-076.
Rebollar, C. J., E. R. Kanasewich, and E. Nyland (1984). Focal depths and source parameters of the Rocky Mountain House earthquake swarm from digital data at Edmonton, *Can. J. Earth Sci.* **21,** 1105–1113, doi: 10.1139/e84-115.
Rydelek, P. A., and I. S. Sacks (1989). Testing the completeness of earthquake catalogues and the hypothesis of self-similarity, *Nature* **337,** 251–253, doi: 10.1038/337251a0.
Schultz, R., V. Stern, and Y. J. Gu (2014). An investigation of seismicity clustered near the Cordel Field, west central Alberta, and its relation to a nearby disposal well, *J. Geophys. Res.* **119,** no. 4, 3410–3423, doi: 10.1002/2013JB010836.
Shi, Y., and B. A. Bolt (1982). The standard error of the magnitude–frequency *b* value, *Bull. Seismol. Soc. Am.* **72,** no. 6, 1677–1687.
Stern, V. H., R. J. Schultz, L. Shen, Y. J. Gu, and D. W. Eaton (2013). Alberta Earthquake Catalogue, Version 1.0: September 2006 through December 2010, *Alberta Geological Survey Open-File Rept. 2013-15*, 36 pp.
Tsai, V. C., B. Minchew, M. P. Lamb, and J. P. Ampuero (2012). A physical model for seismic noise generation from sediment transport in rivers, *Geophys. Res. Lett.* **39,** L02404, doi: 10.1029/2011GL050255.
Vassallo, M., G. Festa, and A. Bobbio (2012). Seismic ambient noise analysis in southern Italy, *Bull. Seismol. Soc. Am.* **102,** no. 2, 574–586, doi: 10.1785/0120110018.
Webb, S. C. (2007). The Earths 'hum' is driven by ocean waves over the continental shelves, *Nature* **445,** 754–756, doi: 10.1038/nature05536.
Wessel, P., and W. H. F. Smith (1998). New, improved version of the Generic Mapping Tools released, *Eos Trans. AGU* **79,** 579–579, doi: 10.1029/98EO00426.
Wetmiller, R. J. (1986). Earthquakes near Rocky Mountain House, Alberta, and their relationship to gas production facilities, *Can. J. Earth Sci.* **23,** 172–181, doi: 10.1139/e86-020.
Wiemer, S. (2001). A software package to analyze seismicity: ZMAP, *Seismol. Res. Lett.* **72,** 373–382, doi: 10.1785/gssrl.72.3.373.
Wiemer, S., and M. Baer (2000). Mapping and removing quarry blast events from seismicity catalogs, *Bull. Seismol. Soc. Am.* **90,** no. 2, 525–530, doi: 10.1785/0119990104.
Wiemer, S., and M. Wyss (2000). Minimum magnitude of complete reporting in earthquake catalogs: Examples from Alaska, the Western United States, and Japan, *Bull. Seismol. Soc. Am.* **90,** 859–869, doi: 10.1785/0119990114.
Wilson, D., J. Leon, R. Aster, J. Ni, J. Schule, S. Grand, S. Semken, S. Baldridge, and W. Gao (2002). Broadband seismic background noise at temporary seismic stations observed on a regional scale in the southwestern United States, *Bull. Seismol. Soc. Am.* **92,** 3335–3341, doi: 10.1785/0120010234.
Withers, M. M., R. C. Aster, C. J. Young, and E. P. Chael (1996). High-frequency analysis of seismic background noise as a function of wind speed and shallow depth, *Bull. Seismol. Soc. Am.* **86,** 1507–1515.
Woessner, J., and S. Wiemer (2005). Assessing the quality of earthquake catalogs: Estimating the magnitude of completeness and its uncertainties, *Bull. Seismol. Soc. Am.* **95,** no. 4, 684–698, doi: 10.1785/0120040007.
Young, C. J., E. P. Chael, M. M. Withers, and R. C. Aster (1996). A comparison of the high-frequency (>1 Hz) surface and subsurface noise environment at three sites in the United States, *Bull. Seismol. Soc. Am.* **86,** 1516–1528.

Zeiler, C., and A. A. Velasco (2009). Seismogram picking error from analyst review (SPEAR): Single-analyst and institution analysis, *Bull. Seismol. Soc. Am.* **99,** no. 5, 2759–2770, doi: 10.1785/0120080131.
Zhu, T., K. Chun, and F. W. Gordon (1991). Geometrical spreading and *Q* of *Pn* waves: An investigative study in eastern Canada, *Bull. Seismol. Soc. Am.* **81,** no. 3, 882–896.

Ryan Schultz
Virginia Stern
Alberta Geological Survey
4999 98 Avenue NW
Edmonton, Alberta
Canada T6B 2X3
ryan.schultz@aer.ca

Yu Jeffrey Gu
University of Alberta
116 Street and 85 Avenue NW
Edmonton, Alberta
Canada T6G 2R3

David Eaton
University of Calgary
2500 University Drive NW
Calgary, Alberta
Canada T2N 1N4

Published Online 11 February 2015